Plant Physiology Preview. Published on February 12, 2010, as DOI:10.1104/pp.109.148742

Running head: APM1 function requires catalytic and interaction domains

Corresponding author:

Wendy Ann Peer

Department of Horticulture

Purdue University

West Lafayette, IN 47907

765-496-7958

peerw@purdue.edu

The catalytic and protein-protein interaction domains are required for APM1 function

Fazeeda N. Hosein, Anindita Bandyopadhyay, Wendy Ann Peer, Angus S. Murphy

Department of Horticulture, Purdue University, West Lafayette, IN 47907

Financial source:

National Science Foundation grant numbers 0820648 and 0521811 to ASM.

Abstract

The M1 metallopeptidase APM1 is essential for embryonic, vegetative, and reproductive development in Arabidopsis. Here we show that, like mammalian M1 proteases, APM1 appears to have distinct enzymatic and protein-protein interaction domains and functions as a homodimer. Arabidopsis seedlings treated with ezetimibe, an inhibitor of M1 protein-protein interactions, mimicked a subset of *apm1* phenotypes distinct from those resulting from treatment with PAQ-22, an inhibitor of M1 catalytic activity, suggesting that the APM1 catalytic and interaction domains can function independently. *apm1-1* knockdown mutants transformed with catalytically inactive APM1 did not prevent seedling lethality. However, *apm1-2* has a functional enzymatic domain but lacks the C-terminus, and transformation with catalytically inactive APM1 rescued the mutant. Overexpression of human IRAP rescued all *apm1* phenotypes, suggesting that the catalytic activity was sufficient to compensate for loss of *APM1* function, while overexpression of catalytically inactive IRAP only rescued *apm1-2*. Increased catalytic activity alone is not sufficient to compensate for loss-of-*APM1*-function, as overexpression of another Arabidopsis M1 family member lacking an extended C-terminus did not rescue *apm1-1*. The protein interactions facilitating enzymatic activity appear to be dependent on the C-terminus of APM1, as transformation with an open reading frame containing an internal deletion of a portion of the C-terminus or a point mutation in a dileucine motif did not rescue the mutant. These results suggest that both the catalytic and interaction domains are necessary for APM1 function, but that APM1 function and dimerization does not require these domains to be present in the same linear molecule.

Introduction

Eukaryotic M1 peptidases regulate a wide range of physiological response and developmental pathways, and play essential roles in embryogenesis, reproduction, cell cycle progression and cell viability (Constam et al., 1995; Brooks et al., 2003; Sanchez-Moran et al., 2004; Lyczak et al., 2006; Matsui et al., 2006; Walling, 2006; Peer et al., 2009). Thus far, two M1 aminopeptidases in *Arabidopsis thaliana* have been characterized. Meiotic Prophase Aminopeptidase1 (MPA1, M1.05.1, At1g63770) is required for correct meiotic recombination in both male and female gametophytes (Sanchez-Moran et al., 2004), and the membrane-associated, puromycin-sensitive aminopeptidase M1 (APM1, M1.10.1, At4g33090) (Murphy and Taiz, 1999a; Murphy et al., 2002) is required for embryonic and seedling development as well as cell cycle progression (Peer et al., 2009). *APM1* loss-of-function alleles show pleiotropic phenotypes including embryonic and seedling lethality, dwarfism, loss of apical dominance, reduced seed yield, aberrant planes of cell division, and cell cycle arrest (Peer et al., 2009). These phenotypes suggest functional analogy between APM1 and mammalian puromycin-sensitive aminopeptidase (PSA), which has been shown to function in both cell cycle progression (Constam et al., 1995) and degradation of MHC peptides (Towne et al., 2008). PSA knockout mice have fewer viable embryos, reduced litter size, and are smaller and less fertile or infertile compared to wild type (Osada et al., 2001a, b; Towne et al., 2008). In *Caenorhabditis elegans,* the APM1/ PSA homolog PAM-1 has been shown to be necessary for oocyte to embryo transition as well as the establishment of anterior-posterior polarity (Lyczak et al., 2006). The catalytic domain of APM1 also shares sequence similarity with the mammalian insulin responsive aminopeptidase/ oxytocinase (IRAP) that processes signaling peptides like tachykinin and oxytocin (Tsujimoto et al., 1992; Herbst et al., 1997; Albiston et al., 2004), leukotriene A4 hydrolase (LT4AH) that activates the leukotriene A4 receptor at the cell surface (Rudberg et al., 2002), and aminopeptidase N (AP-N/CD13), which functions in cell surface uptake of cholesterol (Kramer et al., 2005). However, there are no reports linking these mammalian proteins to cell cycle progression.

M1 peptidases are defined by two motifs in the catalytic domain: a zinc coordination motif HEXXH-(X18)-E and a substrate binding motif GXMEN. Mutation of the zinc coordination motif of M1 proteins decreases or abolishes aminopeptidase activity (Medina et al., 1991; Vazeux et al, 1996; Lausten et al., 2001; Pham et al., 2007). GXMEN is an anionic

coordination motif that recognizes the free N-terminus of substrates that is located 22-32 residues N-terminal to the zinc coordination sequence and distinguishes the M1 aminopeptidase family from other gluzincins (Hooper, 1994; Rawlings and Barrett, 1995). Mutation of the GXMEN motif, particularly the Glu residue, also decreases or abolishes aminopeptidase activity (Vazeux et al., 1998; Luciani et al., 1998; Lausten et al., 2001). Arabidopsis APM1 contains both of these motifs and exhibits enzymatic activity similar to other M1 aminopeptidases (Murphy and Taiz, 1999; Murphy et al., 2002).

Eukaryotic M1 peptidases are either membrane anchored or peripheral membrane proteins containing a hydrophobic interaction domain (Dyer et al., 1990; Cadel et al., 1997; Keller et al., 2004; Peer et al., 2009). Subcellular localization of mammalian M1 peptidases such as IRAP and AP-N is important to their function, and perturbation of their subcellular localization either changes or inhibits their function and is an underlying cause of multiple pathologies (Maianu et al., 2001; Alfalah et al., 2006). Sequence homology comparisons, biochemical analyses, and subcellular localization studies indicate that APM1, like IRAP and AP-N, is membrane-associated (Murphy and Taiz, 1999a; Murphy et al., 2000, 2002; Peer et al., 2009).

A subgroup of mammalian M1 metallopeptidases including IRAP and AP-N contain dileucine and acidic cluster protein interaction domains that function in trafficking events in the endomembrane system and at the plasma membrane (Rasmussen et al., 2000; Katagiri et al., 2002; Cowburn et al., 2006). Dysfunction of protein-protein interactions mediated by the C-terminus of these proteins is implicated in multiple human pathologies including metastasis, tumor cell invasion and angiogenesis (Mina-Osorio and Ortega, 2005). Independent function of M1 interaction domains is suggested by evidence that a functional catalytic domain is not essential to AP-N mediation of viral particle endocytosis and cholesterol at the cell surface (Kramer et al., 2005). However, independent function cannot be generalized, as IRAP-mediated exocytosis of plasma membrane proteins requires a functional catalytic domain (Albiston et al., 2004). Further, comparisons of APM1 with IRAP must be restricted to the catalytic and C-terminal interaction domains, as IRAP regulation of GLUT4 exocytosis requires a unique 110 amino acid N-terminal extension of the protein (Hou et al., 2006) not found in APM1 or other members of the M1 family.

Dimerization mediated by disulfide linkages and non-covalent interactions is a structural feature of the many M1 metallopeptidases (Hesp and Hooper, 1997; Papadopoulos et al., 2000; Ofner and Hooper, 2002). AP-N was reported to form a non-covalent homodimer (Hussain et al., 1981), and IRAP is thought to form covalently-bound homo- and heterodimers (Itoh et al., 1997; Bernier et al., 1998; Matsumoto et al., 2000; Mustafa et al., 2001). Homodimerization is thought to be essential to catalytic activity, although several studies have suggested that it may also play a role in eukaryotic M1 protein trafficking (Danielsen, 1990, 1994).

In Arabidopsis, three loss-of-function alleles have been described. Heterozygous *apm1* mutants are dominant or semi-dominant as they exhibit similar phenotypes (including embryonic abortion, post-germination root arrest, and agravitropic root growth) to those observed in homozygotes (Peer et al., 2009). Almost no *APM1* transcript is detected in *apm1-1*, while *apm1-2* produces a truncated protein containing the catalytic domain but lacking the putative C-terminal protein interaction domain, and *apm1-3*, harbors a point mutation in C-terminal protein interaction domain; all exhibit the same mutant phenotypes (Peer et al., 2009). However, the phenotypes observed are not merely a result of reduced overall hydrolytic capacity, as *apm1-2* exhibits the same phenotypes, but lacks the C-terminal protein interaction domain. Therefore, APM1 appears to require both catalytic and protein-protein interaction domains for full functionality.

While analyses of *apm1* loss-of-function alleles have provided insight into APM1 function, questions regarding the sequence and domain structure of the protein remain outstanding. Here we analyze which structural and functional elements are required for APM1 dimerization and function. We examine whether the HXLXH and GXMEN motifs contribute equally to APM1 function and whether M1 aminopeptidase function is conserved across plant and animal kingdoms. To resolve these questions, we transformed *apm1* mutants with modified forms of the *APM1* open reading frame and analyzed complementation of *apm1* embryo lethal (seed set) and seedling lethal (post-germination root-arrest) phenotypes to dissect the contribution of APM1 subdomains to overall function. We repeated these analyses using selected mammalian and plant M1 constructs to assess the extent of conservation of M1 protein function. The data reported here indicate that (1) APM1 has two functional domains that are required for its activity, (2) APM1 functions as a dimer, and (3) the two domains do not need to be present in the same linear molecule for APM1 functionality.

Results

Sequence comparisons and activity cluster APM1 with PSA/PAM-like M1 proteins

A phylogenetic analysis of M1 amino acid sequences was conducted to place Arabidopsis M1 proteases in an evolutionary context. The M1 family contains members from all kingdoms (except viruses) (Figure 1, Figure S1). In Arabidopsis, there are three canonical M1 aminopeptidases, which have the characteristic M1 aminopeptidase motifs (Rasmussen *et al*. 2000; Murphy *et al*., 2002; Albiston *et al*., 2004): APM1, MPA1 and another M1 aminopeptidase encoded at the locus At5g13520 (Figure S1).

The Meiotic Prophase Aminopeptidase (MPA1, M1.05.1, At1g63770) is most similar to the prokaryotic M1 subfamily (M1.05) (Figure 1A, S1A). MPA1 is expressed in meiocytes, associates with meiotic chromatin, and functions in both male and female meiosis in Arabidopsis (Sanchez-Moran et al., 2004; Pradillo et al., 2007). Shorter and longer isoforms of the protein (M1.05.1.1 and M1.05.1.2) have been identified based on cDNA transcripts. Little is known about the activities of the other canonical M1 aminopeptidase encoded by At5g13520, referred to here as TAF2-LIKE2 (TAF2L2). TAF2L2 contains putative PDZ and nuclear localization motifs and groups most closely to human M1 TAF2 (M1.972), a protein of unknown function named for its partial homology to a TATA binding protein-associated factor (TAF), which function inmodification of transcription factors to facilitate complex assembly and transcription initiation. A non-canonical M1-like protein encoded at the locus At5g52910 also exhibits homology to the human TAF2 protein, but has HEXXH-(X25)-E instead of the canonical HEXXH-(X18)-E in its apparent catalytic domain.

Phylogenetic and biochemical analyses (Murphy and Taiz 1999a; Murphy *et al*., 2002; Smith et al., 2003; http://merops.sanger.ac.uk/) classify APM1 as the single Arabidopsis member of the M1.10 plant-animal (PSA/APM/PAM-1) subfamily of M1 metallopeptidases in Arabidopsis (Figure 1A, S1A). The M1.10 subfamily is closely related to the mammalian cystinyl-AP M1.11 subfamily characterized by IRAP, which mediates interactions with AS160 in GLUT4 trafficking, and ERAP, which functions in N-terminal peptide processing within the endoplasmic reticulum. APM1 exhibits only 24% identity with MPA1 isoforms in the conserved catalytic domain and even less similarity outside of this region. APM1 also contains a PSA/PAM-like C-terminal domain containing putative protein-protein interaction motifs not

found in MPA1 and TAF2L2 (Figure 1B). Although there are no members of the AP-N (M1.01) or IRAP/ERAP (M1.11) subfamilies in Arabidopsis (Figure 1A, S1), APM1 does share a number of sequence identities with AP-N and IRAP not seen in other members of the M1.10 subfamily (Murphy *et al.*, 2002; Figure 1B).

Dimerization of APM1

Some other plant aminopeptidases have been shown to require oligimerization for activity (Matsui et al., 2006). We used reducing and crosslinking reagents to examine potential APM1 oligomerization . Microsomal membranes isolated from 5-d old Arabidopsis were cross-linked using bis (bulfosuccinimidyl) suberate (BS^3). These samples were subjected to SDS-PAGE and western blot analyses, which revealed a ~103 kD band in low concentrations or absence of BS^3, and a ~206 kD band in the presence of 1 mM BS^3. Mass spectrometric sequence analysis of the ~206 kD band identified only APM1 sequences in tryptic fragments, indicating that a homodimer was formed (Figure 2A). To confirm that APM1 forms a dimer, whole microsomal membranes prepared with and without the thiol reducing agent dithiothreitol (DTT) were analyzed via Blue Native PAGE followed by western blotting. This analysis confirmed that APM1 forms a dimer (~206 kD band) *in planta* and that disruption of thiol linkages reduces the protein to monomeric form (~103 kD band, Figure 2B). This suggests that APM1 dimerization or dimer stability involves disulphide bonds.

However, fractions solubilized from Arabidopsis microsomal membranes containing purified APM1 and aminopeptidase P1 (APP1, M24, At4g36760) were previously shown to exhibit increased Tyr aminopeptidase activity when treated with the thiol reducing agent DTT (Murphy *et al*., 2002). Examination of recombinant *APM1 in vitro* translation products synthesized as previously described (Murphy et al., 2002) showed that the aminopeptidase activity against peptide substrates or aminoacyl-fluoromethylcoumarin conjugates was not altered by increasing concentrations of DTT ($P > 0.05$, Table 1). This evidence suggests that APM1 monomers may retain hydrolase activity.

APM1 was originally identified via its affinity for the auxin transport inhibitor 1-napthlythalamic acid (NPA) and its ability to slowly hydrolyze this compound (Murphy and Taiz, 1999a, b; Murphy et al., 2002). NPA is structurally similar to phthalamide inhibitors of M1 enzymatic activity in mammals and plants (Komoda et al., 2001; Murphy et al., 2002;

Kakuta et al., 2003), is able to inhibit APM1 aminopeptidase activity when used at high concentrations, and exhibits increasing inhibition of APM1 activity over time (Murphy and Taiz, 1999a; Murphy et al., 2002). Both northern blot analysis (Murphy et al., 2002) and quantitative real-time PCR analysis (Table 2) showed that *APM1* expression increased significantly after treatment with NPA ($P < 0.001$). SDS-PAGE and western blot analysis of recombinant APM1 produced by short term *in vitro* translation (Murphy et al., 2002) in the presence of NPA indicated that NPA does not directly inhibit APM1 protein synthesis (Figure 2C). However, Pro*APM1*:YFP-APM1 signals in Arabidopsis roots rapidly disappear after treatment with NPA at concentrations much lower than those required to inhibit APM1 enzymatic activity (Peer et al., 2009), and APM1 signals (monomer or dimer) could not be observed in Blue Native PAGE / western blot analyses of microsomal membranes isolated from 5-d Arabidopsis seedlings treated with NPA for 1 hour (Figure 2D). These results suggest that NPA affects APM1 protein stability in addition to enzymatic activity.

Putative protein-protein interaction domains

Critical regions in the C-terminus that are required for APM1 function were determined by mutational analysis of amino acids and domains. To confirm that the C-terminal region is required for APM1 function, a truncated form of APM1, similar to that of *apm1-2*, was generated ($APM1^{\Delta 720\text{-}880}$), transformed into *apm1-1* (+/-) and the transformants were genotyped and analyzed. Transformation with this construct failed to complement post-germination root arrest, lack of apical dominance and embryonic defects in homozygotes, and produced a dominant negative phenotype in heterozygotes, in which the root growth arrest phenotype was not rescued (Figure S2, S3). This supports the hypothesis that amino acid residues in this region of the C-terminus are required for APM1 function throughout development.

Dileucine motifs have been shown to play a role in IRAP protein trafficking through protein-protein interactions (Hou et al., 2006; Watson et al., 2008). Dileucine and similar motifs in APM1 were identified and mutated to alanines to determine whether these motifs mediated APM1 protein-protein interactions. These constructs were under the control of a dexamethasone (Dex) inducible promoter; effects of Dex dosage on the *apm1-1* arrested root growth and embryonic abortion phenotypes in lines with these constructs are shown in Figures S4-S6. Of the 13 motifs identified, only one pair ($LL^{728, 729}$), when mutated, was unable to complement

homozygous *apm1-1* root growth arrest (dead at 5 dag) or embryonic abortion phenotypes (significantly fewer seeds than wild type, $P < 0.05$) (Figure 3A, E; S5). The dosage effects of APM1^{L729A} on *apm1-1* arrested root growth phenotype indicate that the construct was expressed (Figure S4). The remaining 12 mutated dileucine motifs were able to complement the *apm1-1* mutant, and therefore apparently are not critical elements for APM1 function (Figure S5-S6). YFP-APM1^{L729A} transformant roots showed faint membrane and cytosolic YFP signals compared to controls (Figure 3B-D). However, western blot analysis of YFP-APM1^{L729A} microsomal membranes did not show a signal indicating the presence of the protein (Figure S7A), suggesting that the protein may be degraded due to a decrease in protein stability. These results suggest that this dileucine pair is necessary for APM1 function or stability and that LL^{728,729} may also function in conjunction with another protein-protein interaction domain within APM1.

Through bioinformatic analyses we identified four candidate protein-protein interaction domains (see methods). Only one of the internal deletion constructs, APM1$^{\Delta 757\text{-}786}$, in the region most similar to the protein-protein interaction GLUT4/AS160 trafficking domain in the C-terminus of IRAP, was unable to complement homozygous *apm1-1* root growth arrest (dead at 5 dag) or embryonic abortion (significantly fewer seeds than wild type, $P < 0.05$) phenotypes (Figure 3F, J, S5), whereas the other deletion constructs rescued the mutant (Figure S5, S6). These constructs were under the control of a Dex inducible promoter, Dex dosage effects on the *apm1-1* phenotypes are shown in Figure S4. Expression analysis revealed that the *YFP-APM1$^{\Delta 757\text{-}786}$* construct was expressed (Figure S7C). Faint membrane and cytosolic YFP signals were observed in YFP-APM1$^{\Delta 757\text{-}786}$ transformant roots compared to control (Figure 3G-I), and western blot analysis of YFP-APM1$^{\Delta 757\text{-}786}$ microsomal membranes did not show a signal (Figure S7B). These results suggest that, like APM1 ^{L729A}, this mutation results in decreased protein stability. Together these results suggest that these regions of APM1 are involved in protein stability and/or function, which may include protein-protein interactions and/or trafficking of APM1 to the correct location for it to function.

The APM1 catalytic domain is required for development

To investigate the roles of the two APM1 catalytic domains for APM1 function, point mutations in the substrate-binding GAMEN and zinc-binding HELAH motifs were generated by site-

directed mutagenesis. *apm1-1* (+/-) seedlings were transformed with Pro*APM1*:YFP-APM1^{M273K} or Pro*APM1*:YFP-APM1^{H307A} and the resulting transformants were genotyped and analyzed. Both point mutation constructs failed to complement the root growth arrest and embryonic abortion phenotypes in homozygotes (Figure 4A-D). This suggests that the HELAH and the GAMEN motifs are both required for APM1 function. However, it appears that the defect in embryo development and subsequent seed set is partially compensated for by expression of APM1 with an altered GAMEN motif (Figure 4D, S4), suggesting that either substrate specificity or catalytic activity is less important for progression of embryogenesis. Both point mutation transformants exhibited upturned leaf margins in *apm1-1*, although this phenotype was not observed in *apm1-2* (+/-) transformed with these constructs.

In *apm1-2*, a truncated protein (APM1^{R688*}) is generated which includes the catalytic domain, but lacks the protein-protein interaction domain. When *apm1-2* (+/-) was transformed with Pro*APM1*:YFP-APM1^{M273K} or Pro*APM1*:YFP-APM1^{H307A} both constructs were able to complement the arrested root growth, loss of apical dominance, and embryonic abortion and gravitropic response phenotypes of the homozygous mutants (Figure 4 E-H). BS^3 crosslinking showed that both of the catalytically inactive APM1 proteins formed homodimers (~206 kD) as well as heterodimers with APM1^{R688*} (~237 kD) (Figure 4I). Mass spectrometric analysis of BS^3 treated microsomal membranes confirmed that APM1 heterodimers were formed with the mutated APM1 sequences.

M1 catalytic activity alone is not sufficient to rescue *apm1*

The TAF2L2 M1 aminopeptidase possesses the two signature conserved catalytic motifs, but lacks a homologous C-terminal protein-protein interaction domain present in APM1. TAF2L2 has aminopeptidase activity (L. Walling, unpublished data, referenced in Walling, 2006), although its function *in planta* is currently unknown. To determine if additional M1 aminopeptidase activity alone is sufficient to rescue any of the *apm1* phenotypes, *apm1-1* (+/-), *apm1-2* (+/-) and *apm1-3* (-/-), were transformed with full length TAF2L2 cDNA fused to GFP under the control of a 35S promoter (Pro*35S*:GFP-TAF2L2). Overexpression of TAF2L2 did not rescue *apm1-1* or *apm1-2*. However, the resulting *apm1-3* (APM1^{A694V}) Pro*35S*:GFP-TAF2L2 transformants exhibited wild type root length and gravitropic response ($P > 0.05$, Figure S8A, G), although the loss of apical dominance and embryonic abortion phenotypes were not rescued

($P < 0.05$, Figure S8E-F, S4). No change in leaf morphology was observed during vegetative growth (Figure S8B-D). Western blot analysis of BS^3 crossed linked microsomal membranes showed that GFP-TAF2L2 was present as a monomer (~80 kD), a homodimer (~160 kD) and a heterodimer with APM1 (~180 kD) (Figure S8H).

By homology, TAF2L2 also belongs to the TATA binding protein-associated factor family. GFP-TAF2L2 subcellular localization showed GFP signals in the cytosol and nucleus, and nuclear localization was confirmed by co-localization with DAPI (Figure S8I). However, unequivocal microsomal or plasma membrane localization was not observed. Although TAF2L2 was able to form a heterodimer with $APM1^{A694V}$ and rescue the root growth arrest phenotype, the catalytic activity of TAF2L2 alone is not sufficient to compensate for lack of APM1 function.

Catalytic and protein-protein interaction activity are required for APM1 function

Selective M1 protease inhibitors were used to biochemically separate the catalytic and protein interaction activities of APM1. We could thereby assess which *apm1* seedling phenotypes might be attributed to a lack of APM1 hydrolytic activity and which might be more associated with altered C-terminal protein-protein interactions or subcellular trafficking of APM1. Ezetimibe, a mammalian intestinal cholesterol uptake inhibitor, binds the C-terminus of AP-N without inhibiting hydrolytic activity (Kramer et al., 2005). Treatment of wild type seedlings with ezetimibe phenocopied the root and cotyledon defects seen in *apm1-1* (+/-) and *apm1-2* (+/-) (Figure S9A-C). Pro*APM1*:YFP-APM1 subcellular localization in Arabidopsis root tips appeared to be unaltered after ezetimibe treatment compared to untreated controls (Figure S9H, I).

PAQ-22 is an enzymatic inhibitor that specifically inhibits the hydrolytic activity of M1 aminopeptidases and has been shown to inhibit APM1 enzymatic activity (Komoda et al., 2001; Kakuta et al., 2003; Murphy et al., 2002). Wild type seedlings treated with PAQ-22 also exhibited truncated roots, as well as the enlarged hypocotyl cells observed in *apm1* mutants (Figure S9D-G; Peer et al., 2009). However, Pro*APM1*:YFP-APM1 did not appear to be mislocalized in Arabidopsis root tips after PAQ-22 treatment (Figure S9H, J). These results suggest that both the protein-protein interaction and catalytic domains are essential for APM1 function, but inhibiting either activity alone did not alter localization.

Conservation of M1 function between the plant and animal kingdoms

Human IRAP, one of the best characterized members of the M1 metallopeptidase family, and apart from a unique 110 amino acid N-terminus extension, exhibits sequence and enzymatic similarity to APM1. An IRAP cDNA under the control of a 35S promoter was used to transform *apm1-1* (+/-) and rescued all of the *apm1-1* (-/-) phenotypes (arrested root growth, gravitropic response, loss of apical dominance and defects in embryo development) (Figure 5A-C; S4, S10 A-E). This suggests that there is conservation of M1 function between the plant and animal kingdoms. To determine if expression of a catalytically inactive IRAP would rescue any of the *apm1* phenotypes, *apm1-1* (+/-) was transformed with a mutated, catalytically inactive form of an IRAP cDNA (IRAPm) (Ye et al., 2006) under the control of a 35S promoter. This transformation did not rescue the arrested root phenotype, loss of apical dominance or embryonic abortion phenotypes of *apm1-1* homozygotes and heterozygotes (Figure 5A-C) as was the case with transformants created with catalytically inactive APM1 (Figure 4A-D, S3).

Transformation of *apm1-2* (+/-) with either the wild-type cDNA of IRAP or IRAPm was also able to rescue all of the *apm1-2* (-/-) phenotypes (arrested root growth, gravitropic response, loss of apical dominance and defects in embryo development) (Figure 5D-F; S3, S10A-J). A leaf phenotype similar to what was seen with catalytically inactive APM1 transformants was also observed.

In western blot analyses of heterologously expressed IRAP in Arabidopsis, IRAP (~165 kD monomer) was found in microsomal membranes (Figure S10K). Following proteinase K digestion, full-length IRAP was observed in the microsomal membrane fractions (Figure S10K), suggesting that IRAP is a peripheral membrane protein in Arabidopsis. APM1 in wild type is shown for reference in Figure S10L. APM1-IRAP heterodimers formed in *apm1-1* (APM1 - IRAP, ~265 kD) and *apm1-2* (APM1 ^{R668*}- IRAP, ~237 kD), in the absence and presence of BS^3 (Figure S10L), and was confirmed by sequence analysis of the bands by mass spectrometry. This suggests that APM1-IRAP forms a stable heterodimer even in the absence of cross-linking reagent, resulting in rescued *apm1* phenotypes.

To further investigate if the unique N-terminal AS160/GLUT4 protein-protein interaction domain and the transmembrane domain ($IRAP^{1-109}$) were sufficient to rescue of *apm1*, *apm1-1*(+/-) was transformed with a cDNA encoding this region (see Methods) under the control of a 35S promoter. This construct failed to rescue the *apm1* mutant phenotypes (Figure S11A-F),

suggesting that the conserved catalytic and the C-terminal protein-protein interaction domains of IRAP were responsible for the observed activity and likely mediate dimerization with APM1.

An APM1-IRAP chimera was generated where the N-terminal portion of APM1, containing the first 210 amino acid residues, was fused to IRAP, lacking the first 110 amino acid residues. Transformation with this construct rescued homozygous *apm1-1*, confirming that the protein-protein interaction domain of the C-terminus of IRAP can compensate for APM1 function (Figure S11G-K). These results support the hypothesis that the M1 catalytic and the C-terminal protein-protein interaction domain functions are conserved between plants and animals.

Subcellular localization of APM1 is important for its activity

M1 peptidases are either peripheral membrane or membrane anchored proteins (Dyer et al., 1990; Cadel et al., 1997; Keller et al., 2004; Peer et al., 2009). APM1 has previously been shown to be peripherally associated with the plasma membrane and endomembrane structures (cytosolic face) (Murphy et al., 2002; Peer et al., 2009), indicating that it is a peripheral membrane protein. Sequence comparisons were used to identify a conserved N-terminal hydrophobic region in the protein (Figure 1B). An APM1 cDNA in which this putative hydrophobic interacting domain was deleted ($APM1^{\Delta 98\text{-}205}$) was used to transform *apm1-1* (+/-). Transformation with this construct was not able to restore wild type growth or gravitropic response in *apm1-1* homozygote plants (Figure 6A, E, F). Transformants showed a faint YFP cytosolic signal indicative of altered subcellular localization (Figure 6 B-D). These results indicate that this hydrophobic region is required for APM1 membrane association, and therefore subsequent localization to the plasma membrane.

Discussion

The results presented here indicate that APM1 functions as a dimer and requires both catalytic and protein interaction domains for full functionality. As is seen in other M1 proteases (Danielsen, 1990, 1994; Papadopoulos et al., 2000; Ofner and Hooper, 2002; Ye et al., 2006) dimer formation is necessary for enzymatic and/or cellular trafficking of the protein. In the proposed model (Figure S12), native APM1 forms a homodimer and localizes to sites of action on the surface of endomembrane compartments and the plasma membrane (Peer et al., 2009). In *apm1-1* (+/-), some APM1 protein can form a homodimer, but due to the low levels present in

the mutant (Peer et al., 2009), not all of the APM1 protein can dimerize and the residual monomers have cytosolic localization. In *apm1-2* (+/-), in which a truncated form of APM1 is generated ($APM1^{R688*}$), a dimer can form either with itself, ($APM1^{R688*}$-$APM1^{R688*}$), or full length APM1 (APM1-$APM1^{R688*}$). Although the *apm1-2* monomeric truncated protein may be more stable in the cell, the resulting dimers are predicted to be less stable than complete homodimers and would be likely to dissociate more readily.

The C-terminal domains of some mammalian M1 aminopeptidases have been shown to enhance enzymatic activity and also function as intra-molecular chaperones required for correct protein folding and trafficking to the plasma membrane (Ofner and Hooper, 2002; Rozenfeld et al., 2004). APM1 may also have intra-chaperone activity, which may account for the severity of the *apm1-2* phenotype, since *apm1-2* contains a catalytic domain but lacks the C-terminal domain. Chaperone-dependent activation of APM1 may involve additional chaperone activities as APM1 co-purified with the cellular chaperone/ PPIase FKBP42/TWISTED DWARF 1 (TWD1) (Murphy et al., 2002; Geisler et al., 2003) and a strong interaction was observed between APM1 and TWD1 in split ubiquitin and co-immunoprecipitation assays (Lee and Murphy, unpublished).

The hypothesis that the APM1 catalytic domain does not function independently is further supported by a lack of *apm1-1* and *apm1-2* complementation by transformation with a C-terminal deletion construct of APM1 ($APM1^{\Delta 757-786}$), $APM1^{L729A}$, or overexpression of the M1 aminopeptidase TAF2L2 that lacks the C-terminal protein interaction domain. In all cases, a lack of either intact APM1 or a lack of the C-terminal interaction domain in the endogenous or recombinant protein fails to rescue mutant phenotypes. Only in the case of *apm1-3*, which harbors an A>V point mutation in the C-terminus, is partial rescue observed. Rescue cannot be accomplished by increasing catalytic activity alone.

Although both the catalytic and protein interaction domains of APM1 are required for its function, these domains do not need to be in the same linear protein. Only one copy of each is sufficient for APM1 function, as illustrated by the ability of the catalytically inactive forms of APM1 and IRAP to rescue *apm1-2* phenotypes. In the proposed model, when *apm1-1* is transformed with either APM1 or IRAP, the mutant phenotypes are rescued (Figure S12). This can be a result of either the recombinant protein forming homodimers with itself, or in the case of IRAP, forming heterodimers with APM1. When catalytically inactive APM1 or IRAP is

expressed in *apm1-1* (+/-), the mutant phenotype is not rescued, indicating insufficient formation of enzymatically active dimers to rescue the *apm1* phenotype. However, when transformed into *apm1-2*, the catalytically inactive proteins were able to rescue the mutant phenotype, presumably through their ability to form enzymatically active heterodimers with the truncated protein (Figure S12). Mutations in APM1 which alter its subcellular localization result in an inability to rescue *apm1* phenotypes, highlighting localization as an important factor in the function of APM1.

Conclusions

The severe morphological and cell cycle defects observed in *apm1* mutants, the lack of mutant rescue by overexpression of conserved M1 catalytic domains, and the association of APM1 with important membrane signaling complexes suggest that APM1 is not merely a component of the protein turnover machinery of plant cells. APM1 and MPA1 appear to function analogously with animal M1 peptidases that act in protein and peptide hormone maturation / degradation as well as regulation of embryogenesis, reproduction, meiotic and mitotic cell cycle progression, and cell viability. Activity and correct localization of APM1 in these processes appear to require dimerization events mediated by the C-terminal protein interaction domain. Finally, the results presented here suggest that APM1 function is more analogous to PSA/PAM1/AP-N than in an IRAP and suggest that a mechanism analogous to the IRAP/GLUT4 interaction does not occur in plants. Future studies will determine the targets and partners of APM1 that are downstream regulators or structural components of developmental processes.

Methods and materials

Phylogenetic analysis

To identify all M1 aminopeptidase sequences in the Arabidopsis (*Arabidopsis thaliana*) genome and in other fully or partially sequenced genomes, non-redundant protein sequences with the M1 protein sequence in their definition fields were obtained from GenBank (Benson *et al*., 2000). Arabidopsis non-redundant protein sequences were also blasted using subdomains of APM1 and MPA1. All alignments were performed using the default parameters in (MEGA Kumar, Tamura, and Nei, 2004) [Pairwise alignment, with a Gap Opening Penalty of 10 and Gap Extension Penalty 0.1. Multiple Alignment, with a Gap Opening Penalty of 10 and Gap Extension Penalty 0.2. Protein Weight Matrix Gonnet. Residue-specific Penalties ON, Hydrophilic Penalties ON,

Gap Separation Distance of 4 End Gap Separation OFF Negative Matrix OFF and Delay Divergent Cutoff (%) of 30], which uses ClustalW as a base alignment algorithm (Thompson *et al*., 1994): Matrix: Gonnet250, Gapopen: 10, No endgap: yes, Gap ext: 0.2, Gap dist: 4, Iteration: 1, Numiter: 1, Output format: Phylip, Output order: aligned, Tree type: Phylip, Correct dist.: off, Ignore gaps: off, Clustering: NJ. Files were converted to the nexus format and ran it in MrBayes using ngen=1000000, aamodel=fixed, samplefreq=100. Alignments were to generate unrooted neighbor joining trees, also using the default parameters [Bootstrap of 1000 and random seed of 4148, complete deletion of gaps and missing data and using Poisson correction for the amino acid model] to $P < 0.01$The alignments calculated bootstrapping values and only used genes for which transcripts were available. Current MEROPS alignments were assembled in consultation with the authors of this manuscript. Our approach also contained structural characterization modeled on mammalian PSA to determine the validity of the alignment based on helices and catalytic sties.

Growth conditions

Seedlings were grown on 1% phytagar plates, ¼ Murashige and Skoog (MS) basal salts, pH 5.5, 22°C and 14 h, 100 μmol m^{-2} s^{-1} except as indicated for specific treatments. *apm1* mutants were transferred to 1% phytagar plates, ¼ MS basal salts, pH 5.5, supplemented with 0.5% sucrose to induce adventitious root formation from the hypocotyls prior to transfer to soil; however, a robust root system is never formed. Growth conditions for plants on soil were grown in the greenhouse under natural light conditions, and in the winter the day length was extended to 16 hours with HID lights (150 μmol m^{-2} s^{-1}). See http://www.hort.purdue.edu/hort/facilities/greenhouse/hlaTech.shtml for more information.

Generation of constructs

Site-directed mutagenesis was carried out by generation of two fragments which were then used in a three-way ligation reaction to generate either Pro*35S*:APM1-YFP or Pro*APM1*:YFP-APM1 with the mutated catalytic site, G273K or H307A. In this procedure, one of the two mutagenic primers and one of the external primers where used to amplify the PCR products. All PCR-derived products were sequenced completely for correct sequence determination: gene specific forward primer 5’ GAT TCT TCC CCA TGG AGT GGG 3’ (Nco I restriction site); gene

specific reverse primer 5' GCG CTT TTC ATA TGA ACC ACA AC 3' (Nde I restriction site). To generate the G273K construct the following primers were used 5' GCC GGC GCT AAG GAG AAT TAT 3' and 5' ATA ATT CTC CTT AGC GCC GG C 3', while the H307A construct was generated using 5' GGC CAG TTC TGC AGC AAC TAC 3' and 5'GTA GTT GCT GCA GAA CTG GCC 3' primers. These constructs were then transformed into *Agrobacterium tumafaciens* C58 pGV3850 (Zambrisky *et al*., 1983) by electroporation. The *apm1-1* (+/-) and *apm1-2* (+/-) mutants were transformed by the floral dip method (Clough and Bent, 1998), and transformants were selected using Basta (50 ppm) and genotyped for the *apm1-1* T-DNA mutation or the *apm1-2* point mutation as follows. PCR with Lba1 primer 5'TGG TTC ACG TAG TGG GCC ATC G 3' and 5' TGA TGA AGC TAC GTC CAA CAT GGC GG 3' were used to determine if the transformant contained a T-DNA mutation. To determine if the seedling was homozygous for the T-DNA mutation, PCR with primers 5' TGA TGA AGC TAC GTC CAA CAT GGC GG 3' and 5' CTT TTA TAA TAC GAG GGT TGT AAG C 3'were used. To determine if the transformant contained the point mutation (*apm1-2*), an amplicon was generated using gene specific primers (5' TTC ATT GGC GTT TTC CAG TTT GCT G 3' and 5' TTA CAC CGG AAA GTC CAT AAA GTC 3', and subsequently digested using Xmn I. (This mutation resulted in a loss of Xmn I restriction site). Seventeen independent lines were isolated for both constructs and all seventeen exhibited similar phenotypes. Three were used for detailed phenotypic analyses.

A truncated form of APM1 (APM1Δ720-880) was generated by digesting Pro35S:*YFP-APM* (Peer *et al*., 2009) with BstB1 and Blp1, blunt-ending and subsequently self-ligated. To generate APM1$^{\Delta 98\text{-}205}$, an internal deletion of APM1 was amplified by PCR from APM1 cDNA using the primers 5' CCA TGG TTT GTT TGA CTA CGT GG 3' with an Eco R1 site and 5' GAA TTC CAT CGG ATG TAT GAT CTT CCA CG 3' with a Nco I site. This fragment was subcloned into Pro35S:*YFP-APM* construct (Peer *et al*., 2009). Constructs were transformed into plants, and plants were screened and genotyped as above. Five independent lines were isolated for Pro*35S*:*YFP-APM1*$^{\Delta 720\text{-}880}$ and all five exhibited similar phenotypes. Three were used for detailed phenotypic analyses. Two independent lines were isolated for Pro*35S*:*YFP-APM1*$^{\Delta 98\text{-}205}$ and both exhibited similar phenotypes, with one line exhibiting a stronger signal when viewed under the confocal microscope. This line was used for detailed phenotypic analyses.

Point mutations of the dileucine resides and internal deletions of the putative protein/protein interaction domains were generated using primers (Table S1), subcloning corresponding fragments in pENTR:*YFP-APM1* and subsequently into pOpOn2.1 using reagents and protocols from Invitrogen (Carlsbad, California, USA). Constructs were transformed into plants, and plants were screened and genotyped as above. For all constructs, at least six independent lines were isolated and all exhibited similar phenotypes. Four lines were used for detailed phenotypic analyses.

A full-length IRAP cDNA was amplified by PCR from pCI-IRAP (Albiston *et al*., 2004) using the primers 5' CACCATGAATAGAAGCTCAGGCCTTCGG3 ' and 5' CTACAGCCACCATGTGAGACTTTTGAGG 3', then subcloned into pENTR-D/TOPO and subsequently into the Gateway binary vector pGWB15 using reagents and protocols from Invitrogen (Carlsbad, California, USA). The same procedure was employed for the catalytically inactive form of IRAP (Albiston *et al*., 2004). Constructs were transformed into plants, and plants were screened and genotyped as above. Five independent lines were isolated for Pro*35S*:*IRAP* and Pro*35S*:*IRAPm* and all exhibited similar phenotypes. Three lines were used for detailed phenotypic analyses.

The N-terminus of IRAP (1-109) was amplified by PCR from pCI-IRAP IRAP (Albiston *et al*., 2004) using the primers 5' AAA AAG CAG GCT GGA TGA ATA GAA GCT C 3' and 5' AGA AAG CTG GGT TTA GAA TGT CAT CGA GG 3', which was subcloned into pDONR Zeo and subsequently into the Gateway binary vector pEARLEYGATE 104 using reagents and protocols from Invitrogen (Carlsbad, California, USA). Constructs were transformed into plants, and plants were screened and genotyped as above. Four independent lines were isolated for Pro*35S*:*IRAP* (1-109) and all exhibited similar phenotypes. Three lines were used for detailed phenotypic analyses.

The chimera between APM1 and IRAP was generated. Two fragments were generated using PCR as follows: The first fragment was generated using 5' GAA TTC ATG GAT CAG TTC AAA GG 3' (EcoR1 restriction site) and 5' GGA TCC TTG ATA GGA GAC AAT C 3' (BamHI restriction site) were used to amplify the first 210 amino acid residues. The second fragment was generated using 5' GAA TCC TTC AGG GGT TCT GTG AC 3' (Bam HI restriction site) and 5' CCC GGG CTA CAG CCA CCA TGT G 3' (Xma I restriction site) to amplify the region the CDS of IRAP without the first 110 amino acid residues. These fragments

were subcloned into pBI121 in a three-way ligation reaction. Constructs were transformed into plants, and plants were screened and genotyped as above. Eight independent lines were isolated for Pro*35S*:*YFP-APM1*Δ98-205 and all exhibited similar phenotypes. Three lines were used for detailed phenotypic analyses.

A full-length At5g13520 cDNA was amplified by PCR from pUNI-At5g13520 using the primers 5' AGAAAGCTGGGTTTAGATGTACTTAG 3 ' and 5' CTACAGCCACCATGTGAGACTTTTGAGG 3', then subcloned into pDONR/ZEO and subsequently into the Gateway binary vector pEARLEYGATE 104 using reagents and protocols from Invitrogen (Carlsbad, California, USA). Constructs were transformed into plants, and plants were screened and genotyped as above. Transformants from *apm1-3* were genotyped as follows: an amplicon was generated using gene specific primers (5' TTC ATT GGC GTT TTC CAG TTT GCT G 3' and 5' TTA CAC CGG AAA GTC CAT AAA GTC 3', and subsequently digested using AluI. (This mutation resulted in a loss of Alu I restriction site). Three independent lines were isolated for Pro*35S*:*YFP-APM1*$^{\Delta 98\text{-}205}$ and all exhibited similar phenotypes. All three lines were used for detailed phenotypic analyses.

Inducible constructs

Point mutation of the dileucine residues were generated as follows: dileucine residues were identified and primers were mutated to selected leucine residues to alanine residues using Primer Generator (http://www.med.jhu.edu/medcenter/primer/primer.cgi) (Table S1). These primers were used to generate mutagenic fragments and were subcloned into pENTR-TOPO/D YFP-APM1 (Peer *et al*., 2009), using the unique restriction sites generated with each point mutation. Point mutations that were after the first 300 amino acid residues, used the following primer combinations to generate the mutagenic fragments: Forward primer 5' GAT TCT TCC CCA TGG AGT GGG 3' (Nco I restriction site) and reverse primer 5' TTA GTT TGA AGA GAG CTG AGC AAC G 3' (Blp I restriction site). Point mutations that were before the first 300 amino acid residues, used the following primer combinations to generate the mutagenic fragments: Forward primer 5' GGA ATT CAT GGA TCA GTT CAA AGG TGA GCC 3' (EcoR1 restriction site) and reverse primer 5' GCG CTT TTC ATA TGA ACC ACA ACA C 3' (Nde 1 restriction site). These fragments were then subcloned into pENTR-TOPO/D YFP-APM1 in a three-way ligation reaction (Peer *et al*., 2009) and subsequently subcloned into gateway

binary vector pOpON2.1 using reagents and protocols from Invitrogen (Carlsbad, California, USA). These were subsequently subcloned into pOpON using reagents and protocols from Invitrogen (Carlsbad, California, USA). Constructs were transformed into plants, and plants were screened and genotyped as above. Resulting transformants were selected on ¼ MS plates supplemented by kanamycin (50 mg ml^{-1}) and genotyped as described above.

Dexamethasone (Dex) was dissolved in either dimethylsulfoxide (DMSO) or ethanol and kept as a 20 mM stock at -20°C. Unless otherwise stated, 10 µM Dex was used for experiments. Dex was added to ¼ MS media with 1% (w/v) phytagar, pH 5.5 plates, to achieve induction during seed germination or after seedling transfer in sterile conditions. For application to soil grown plants, transgenic plants carrying the inducible construct were watered with varying concentrations of Dex (0-10 µM) every 3 days.

Transgenic seeds [*apm1-1* (+/-) transformed with pOpON *YFP-APM*] were sown on plates supplemented with 10 µM Dex (as outlined above) and everyday, 10-20 seedlings were transferred plates without Dex, for 5 days. 6-d seedlings were imaged using a NIKON SMZ-U research grade stereo microscope. The reciprocal experiment was repeated where transgenic seeds were sown on plates without Dex and everyday, 10-20 seedlings were transferred to plates with 10 µM Dex, for 5 days. These experiments were repeated three times, using three lines each time.

Identification of candidate protein-protein interaction domains

Candidate protein-protein interaction domains were indentified using prediction programs which first identified hydrophobic regions in the C-terminus of APM1, which were further analyzed for putative protein-protein interaction sites. Initial identification of the three hydrophobic regions were carried out using prediction programs; Phobius prediction program identified a region between 803-822 as a possible candidate (K□ll *et al*., 2004) and Predict Protein which identified regions between 692-706 and 821-835 (Rost *et al*., 2004). A fourth region (757-786) was identified due to it being most similar to the GLUT4 trafficking domain located in the N-terminal region of IRAP. These regions were compared to results obtain from Predict Protein, which identified putative protein-protein interaction motifs, using the default settings, (stretch = 5, crowd predictions = 7, gap = 8 and itr = 51). Since these putative interaction regions contained protein-protein interaction motifs, they were subsequently targeted for deletion analyses. These

regions were deleted using primers (Table S1), which were used to generate fragments with Xma I restriction sites at either end, with 5' GTTCTCCTGGGGAAGGACAA 3' and 5' TTAGTTTGAAGAGAGCTGAGCAACG 3'. These fragments were then subcloned into pENTR-TOPO/D YFP-APM1 in a three-way ligation reaction (Peer *et al.*, 2009) and subsequently subcloned into pOpON using reagents and protocols from Invitrogen (Carlsbad, California, USA). Transgenic plants were generated as outlined above. Other domain analyses: (NCBI conserved domains http://www.ncbi.nlm.nih.gov/Structure/cdd/wrpsb.cgi?RID=9AZGSHK4014&mode=all and WoLFPSORTII http://wolfpsort.org/results/pa47e8359bfb59d24baa870103166382a.detailed1.html#queryProtein.

Expression analysis

Quantitative real-time PCR analysis of APM1 expression in 5-d NPA treated seedlings

RNA was extracted with the RNeasy kit (Qiagen) from 5 day old seedlings. cDNA was prepared from total RNA with Bioscript Reverse Transcriptase (Bioline). Transcript levels were determined on a Bio-Rad iCycler IQ using iQ^{TM} Sybr © Green Supermix (Bio-Rad) in 20-µL reactions. An aliquot of the RT reaction was used as template. PCR conditions were as follows: 1.5 min at 95°C (one cycle); 30 s at 95°C, 30 s at 54°C, and 30 s at 72°C (45 cycles). Gene-specific primers used were as follows 5' TTTTGGCTGATAGGAACACT 3' and 5' GTGAAGTAGCTTGGAAATGG 3'. Each RT sample was assayed in triplicate. Data were further analyzed in Excel. Transcript levels were normalized to β-tubulin 6 (efficiency 1.07) and GADPH (efficiency 1.05), and quantitated using Pfaffl (2001).

Expression analysis of APM1 in dexamethasone inducible constructs

RNA was extracted with the RNeasy kit (Qiagen) from 5 day old seedlings grown on Dex (Peer et al., 2009). cDNA was prepared from total RNA with Bioscript Reverse Transcriptase (Bioline) from YFP-APM1, APM1^{L729A}, and APM1$\Delta^{757-786}$ lines. Since *APM1* is expressed in these lines, albeit at a low level, it was not possible to use quantitative real-time PCR since this method cannot distinguish between the endogenous transcript and the transgene simultaneously. APM1 and APM1$^{\Delta757-786}$ can be distinguished by electrophoresis since APM1$^{\Delta757-786}$ produces a shorter transcript; however, the point mutation cannot be distinguished from the wild type transcript.

Mass spectroscopy analyses

Mass spectroscopy analyses were as described in Titapiwatanakun et al. (2009).

Microscopy

5-d old seedlings were imaged on a LSM710 confocal laser scanning microscope as outlined in Peer *et al*. (2009). For DAPI staining, seedlings were incubated in DAPI (1 mg ml^{-1}) for 5 minutes, rinsed three times in water before being visualized on the LSM710-META confocal laser scanning microscope.

Gravitropism assay

For analyzing the response to a gravity stimulus 5-d old seedlings were gravistimulated by rotating the plate by 90° for 30 min. To analyze the response of the transgenic plant to a gravity stimulus, seedlings were grown on ¼ MS media with 1% (w/v) phytoagar, pH 5.2 for 5 days (unlike assays conducted at 4 days in Peer *et al*., 2009). Plates were kept in a vertical position. After reorienting the plates by 90°, the root tip position was marked every 3 hours over a 24 hour time period. The angles of curvature were measured by Image J program and the data were analyzed by Microsoft Excel. The averages were calculated from 50-68 seedlings.

Inhibitor studies

For inhibitor studies, wild type, *apm1-1* (+/-) and *apm1-2*(+/-) seedlings were germinated on ¼ MS (pH 5.5), 1% phytagar plates supplemented with either 10 nM PAQ-22 or 50 nM ezetimibe (Zetia®). 5-d old seedlings were imaged using a Nikon-E800 microscope. For NPA assays, seedlings were grown as above for days, then transferred to plates containing 30 µM or 50 µM NPA for 1 hour prior to microsomal membrane preparation as described in Peer *et al*., (2009).

Cross-linking

Microsomal membrane preparations were isolated, without reducing agent, as outlined in Peer *et al*., 2009 and were cross-linked to bis (sulfosuccinimidyl) suberate, BS^3, as outlined in manufacturer's instructions (Pierce Biotechnology, IL, USA). The proteasome inhibitor, MG132, was included in the grinding buffer to ensure that proteolysis was not a factor affecting dimerization. This method was used in analyses of AUX/IAA proteins to prevent degradation

(Gray et al., 2001).Stock solutions of 0.1 mM, 1mM and 10mM were prepared in water which was then added to the membrane preparations to final concentrations of 0.01 mM, 0.1mM and 1mM respectively. Samples were incubated for 2 hours on ice with 1µM MG132, before being quenched with 30mM Tris pH 7.5 for 10 minutes on ice. Samples were then run on SDS-PAGE (sodium dodecyl sulfate polyacrylamide gel electrophoresis) or Blue Native Gel followed by western blot analyses as outlined in Peer *et al*., 2009.

Proteinase K digestion

Microsomal membrane preparations were isolated and digested with proteinase K (100 µg ml^{-1}) (Sigma, St. Louis, MO, USA) for 1 hour on ice. PMSF (phenylmethylsulphonyl fluoride, to a final concentration of 1 mM) was added to terminate the reaction with incubation for 20 minutes on ice. Samples were ran on 8% SDS-PAGE gel followed by western blot analyses with anti-HA (Santa Cruz. Biotechnology, California), (1:500 dilution in 5% skim milk in TBS, 0.1% Tween-20, 16 hr, 4° C) followed by incubation with the secondary antibody (1: 5000, 1 hr , room temperature) and incubation with ECL (Pierce, Rockford IL) for 5 min.

Blue Native PAGE analyses

Microsomal membrane preparations were isolated, with and without reducing agent, as outlined in Peer *et al*., 2009. Membrane preparations were ran on Blue Native PAGE Novex 4-16% Bis-Tris gradient gel (Invitrogen, Carlsbad, CA) as outlined in manufacturer's instructions (Invitrogen, Carlsbad, CA). Western blot analyses were carried out as outlined in Wittig *et al*. (2006), using the APM1 antibody generated in Murphy *et al*. (2002) as outlined in Peer *et al*. (2009). Blots were incubated using α-GFP (Santa Cruz Biotechnology, California), (1:1000 dilution in 5% skim milk in TBS, 0.1% Tween-20, 16 hr, 4°C) followed by incubation with the secondary antibody (1: 5000, 1 hr, room temperature) and incubation with ECL (Pierce, Rockford IL) for 5 min.

In vitro translation

In vitro translation was as described in Murphy et al. (2002). Enzymatic assays were performed as in Murphy and Taiz (1999b) and Murphy et al. (2002), except that PITC (phenylisothiocyante) derivatization in tripeptide hydrolysis assays were replaced with Accutag and peptides were

incubated for only 15 minutes. Protein was incubated in dithiothreitol (DTT) solution indicated for 1h, 6° C before assay. DTT was also present in the assay buffer. The baseline is empty vector control protein in the same buffer.

Accession numbers

Arabidopsis thaliana APM1 (At4g33090), *Neosartorya fischeri* XP_001267120, *Aspergillus fumigatus* XP_751922.1, *Aspergillus clavatus* XP_001271795.1, *Aspergillus niger* CAC_38353.1, *Ashbya gossypii* NP_982415.1, *Pichia stipitis* XP_001385797.2, *Phylloctachys angusta* AAL83915.1, *Saccharomyces cerevisiae* AAG01326.1, *Physcomitrella patens* PP_11099_C2, *Oryza sativa* Os090362500, *Oryza sativa* Os02g0218200, *Dictyostelium discoideum* XP_646344.1, *Danio rerio* XP 684042, *Homo sapiens* PSA NM_006310, *Caenorhabditis elegans* PAM-1 NP_001023210, *Xenopus laevis* NP_001072690.1, *Rattus norvegicus* EDM05852.1, *Aedes aegypti* EAT34883.1, *Drosophila pseudoobscura* XP_001354254.1, *Drosophila melanogaster* AAG48733.1, *Trypanosoma cruzi* strain XP_809697.1, *Homo sapiens* AP-N X13276 , *Homo sapiens* IRAP D50810, *Homo sapiens* ERAP NP 057526, *Rattus norvegicus* VP165 NP 001106874, *Candiditus nitrosopumilus maritimus* ZP_02023923.1, *Cenarchaeum symbiosum* A ABK77113.1, *Oryza sativa* Os03g0819100, *Aspergillus fumigatus* XP_751922, *Aspergillus terreus* XP_001214491, *Aspergillus oryzae* XP_001821168, *Penicillium marneffei* XP_002150453, *Sclerotinia sclerotiorum* XP_001594581, *Botryotinia fuckeliana* XP_001548342, *Podospora anserina* XP_001908716, *Neurospora crassa* XP_959172, *Coccidiodes immitis* XP_001241125, *P. marneffei* XP_002149108, *Aspergillus fumigatus* XP_747910, *N. fischeri* XM_001266098, *Aspergilius nidulans* XP_661886, *Aspergillus niger* XP_001393995, *Aspergillus terreus* XP_001216601, *Cenarchaeum symbiosum* A YP_875417.1, *Candidatus nitrosopumilus maritimus* SCM1 YP_001582291.1, *Bos taurus* AAB28170.1, *Bos taurus* NP 776523.2, *Homo sapiens* AAH06199.3, *Homo sapiens* AAD17527.1, *Homo sapiens* CAG33409.1, *Homo sapiens* NP_056991.2, *Homo sapiens* TAF2 EAW91993.1, *Arabidopsis thaliana* TAF2L2 At5g13520, *Arabidopsis thaliana* MPA1 At1g63770, *Arabidopsis thaliana* At5g52910, *Arabidopsis thaliana* At4g29490, *Arabidopsis thaliana* At1g73960, *Arabidopsis thaliana* At4g36760, *Arabidopsis thaliana* At2g45240, *Arabidopsis thaliana* At1g13270, *Lycopersicon esculentum* AAO15916.1, *Arabidopsis thaliana* At2g24200

Supporting Data

Literature Cited

Albiston, A. L., Ye, S., and Chai, S. Y. (2004). Membrane bound members of the M1 family: More than aminopeptidases. *Protein and Peptide Letters* **11**:491-500.

Alfalah M, Krahn MP, Wetzel G, von Hörsten S, Wolke C, Hooper N, Kalinski T, Krueger S, Naim HY, Lendeckel U. (2006). A mutation in aminopeptidase N (CD13) isolated from a patient suffering from leukemia leads to an arrest in the endoplasmic reticulum. J Biol Chem 281: 11894-1900.

Bernier, S. G., Bellemare, J. M., Escher, E. and Guillemette, G. (1998). Characterization of AT4 receptor from bovine aortic endothelium with photosensitive analogues of angiotensin IV. *Biochem* **37**:4280-4287.

Brooks, D.R., Hooper, N.M., and Isaac, R.E. (2003). The *Caenorhabditis elegans* orthologue of mammalian puromycin-sensitive aminopeptidase has roles in embryogenesis and reproduction. *J Biol Chem* **278**:42795-42801.

Cadel, S., Foulon, T., Viron, A., Balogh, A., Midol-Monnet, S., Noel, N., Cohen, P. (1997). Aminopeptidase B from the rat testis is a bifunctional enzyme structurally related to leukotriene-A_4 hydrolase. *Proc Natl Acad Sci USA.* **94**:2963–2968.

Clough, S., J., Bent, A., F. (1998). Floral dip: a simplified method for *Agrobacterium* mediated transformation of *Arabidopsis thaliana*. *Plant J.* **16**:735–743

Constam, D.B., Tobler, A.R., Rensing-Ehl, A., Kemler, I., Hersh, L.B., and Fontana, A. (1995). Puromycin-sensitive aminopeptidase. Sequence analysis, expression, and functional characterization. *J Biol Chem* **270**: 26931–26939.

Cowburn, A.S., Sobolewski, A., Reed, B.J., Deighton, J., Murray, J., Cadwallader, K.A., Bradley, J.R., and Chilvers, E.R. (2006). Aminopeptidase N (CD13) regulates tumor necrosis factor-alpha-induced apoptosis in human neutrophils. *J Biol Chem* **281**:12458-12467.

Danielsen, E. M. (1990). Perturbation of intestinal microvillar enzyme biosynthesis by amino acid analogs. Evidence that dimerization is required for the transport of aminopeptidase N out of the endoplasmic reticulum. *J Biol Chem* **265**:14566-14571.

Danielsen, E. M. (1994). Dimeric assembly of enterocyte brush border enzymes. *Biochem* **33**:1599-1605.

Dyer, S., H., Slaughter, C., A., Orth, K., Moomaw, C., R. and Hersh, L., B. (1990). Comparison of the soluble and membrane-bound forms of the puromycin- sensitive enkephalin-degrading aminopeptidases from rat. *J Neurochem* **54**:547- 554.

Geisler M, Kolukisaoglu HU, Bouchard R, Billion K, Berger J, Saal B, Frangne N, Koncz-Kalman Z, Koncz C, Dudler R, Blakeslee JJ, Murphy AS, Martinoia E, Schulz B. (2003). TWISTED DWARF1, a unique plasma membrane-anchored immunophilin-like protein, interacts with Arabidopsis multidrug resistance-like transporters AtPGP1 and AtPGP19. Mol Biol Cell ;14: 4238-4249.

Gray, W.M., Kepinski, S., Rouse, D., Leyser, O., Estelle, M. (2001). Auxin regulates SCF(TIR1)-dependent degradation of AUX/IAA proteins. *Nature* **414**:271-276.

Hesp, J. R. and Hooper, N. M. (1997). Proteolytic fragmentation reveals the oligomeric and domain structure of porcine aminopeptidase A. *Biochem* **36**:3000-3007.

Herbst, A., Wolner-Hanssen, P., and Ingemarsson, I. (1997). Risk factors for acidemia at birth. *Obstet Gynecol* **90**: 125-130.

Hou JC, Suzuki N, Pessin JE, Watson RT. (2006). A specific dileucine motif is required for the GGA-dependent entry of newly synthesized insulin-responsive aminopeptidase into the insulin-responsive compartment. J Biol Chem 281: 33457-33466.

Hussain, M. M., Tranum-Jensen, J., Noren, O., Sjostrom, H. and Christiansen, K. (1981). Reconstitution of purified amphiphilic pig intestinal microvillus aminopeptidase. Mode of membrane insertion and morphology. *Biochem J* **199**:179-186.

Itoh, C., Watanabe, M., Nagamatsu, A., Soeda, S., Kawarabayashi, T. and Shimeno, H. (1997). Two molecular species of oxytocinase (L-cystine aminopeptidase) in human placenta: purification and characterization. *Biol Pharm Bull* **20**:20-24.

Katagiri, H., Asano, T., Yamada, T., Aoyama, T., Fukushima, Y., Kikuchi, M., Kodama, T., and Oka, Y. (2002). Acyl-coenzyme a dehydrogenases are localized on GLUT4-containing vesicles via association with insulin-regulated aminopeptidase in a manner dependent on its dileucine motif. *Molecular Endocrinology* **16**:1049-1059.

Keller, S., K. (2004). Role of the Insulin-Regulated Aminopeptidase IRAP in Insulin Action and Diabetes *Biol. Pharm. Bull* **27**:761-764.

Kramer, W., Girbig, F., Corsiero, D., Pfenninger, A., Frick, W., Jahne, G., Rhein, M., Wendler, W., Lottspeich, F., Hochleitner, E.O., Orso, E., and Schmitz, G. (2005).

Aminopeptidase N (CD13) is a molecular target of the cholesterol absorption inhibitor ezetimibe in the enterocyte brush border membrane. *J Biol Chem* **280**:1306-1320.

Komoda M, Kakuta H, Takahashi H, Fujimoto Y, Kadoya S, Kato F, Hashimoto Y (2001). Specific inhibitor of puromycin-sensitive aminopeptidase with a homophthalimide skeleton: identification of the target molecule and a structure-activity relationship study. *Bioorg Med Chem* **9**: 121–131.

Luciani N, Marie-Claire C, Ruffet E, Beaumont A, Roques BP, Fournié-Zaluski MC. (1998). Characterization of Glu350 as a critical residue involved in the N-terminal amine binding site of aminopeptidase N (EC 3.4.11.2): insights into its mechanism of action. Biochemistry 37: 686-692.

Lyczak, R., Zweier, L., Group, T., Murrow, M.A., Snyder, C., Kulovitz, L., Beatty, A., Smith, K., and Bowerman, B. (2006). The puromycin-sensitive aminopeptidase PAM-1 is required for meiotic exit and anteroposterior polarity in the one-cell *Caenorhabditis elegans* embryo. *Dev* **33**: 4281-4292.

Maianu L, Keller SR, Garvey WT. (2001). Adipocytes exhibit abnormal subcellular distribution and translocation of vesicles containing glucose transporter 4 and insulin-regulated aminopeptidase in type 2 diabetes mellitus: implications regarding defects in vesicle trafficking. J Clin Endocrinol Metab 86: 5450-5456.

Matsui M, Fowler JH, Walling LL. (2006). Leucine aminopeptidases: diversity in structure and function. Biol Chem 387: 1535-1544.

Matsumoto, H., Rogi, T., Yamashiro, K., Kodama, S., Tsuruoka, N., Hattori, A., Takio, K., Mizutani, S. and Tsujimoto, M. (2000). Characterization of a recombinant soluble form of human placental leucine aminopeptidase/oxytocinase expressed in Chinese hamster ovary cells. *Eur J Biochem* **267**:46-52.

Medina, J.F, Rådmark, O. Funk C.D., and Haeggström, J.Z. (1991). Molecular cloning and expression of mouse leukotriene A_4 hydrolase cDNA. *Biochem. Biophys. Res. Commun.* **176** : 1516–1524.

Mina-Osorio, P., and Ortega, E. (2005). Aminopeptidase N (CD13) functionally interacts with FcgammaRs in human monocytes. *J Leukoc Biol* **77**: 1008-1017.

Murphy, A., and Taiz, L. (1999a). Localization and characterization of soluble and plasma membrane aminopeptidase activities in Arabidopsis seedlings. *Plant Physiology and Biochemistry* **37**:431-443.

Murphy, A., and Taiz, L. (1999b). Naphthylphthalamic acid is enzymatically hydrolyzed at the hypocotyl-root transition zone and other tissues of Arabidopsis thaliana seedlings. *Plant Physiology and Biochemistry* **37**:413-430.

Murphy, A., Peer, W.A., and Taiz, L. (2000). Regulation of auxin transport by aminopeptidases and endogenous flavonoids. *Planta* **211**:315-324.

Murphy, A., S., Hoogner, K., R., Peer, W., A., and Taiz, L. (2002). Identification, purification, and molecular cloning of N-1-naphthylphthalmic acid-binding plasma membrane-associated aminopeptidases from Arabidopsis. *Plant Physiol* **128**:935-950.

Mustafa, T., Chai, S. Y., Mendelsohn, F. A., Moeller, I. and Albiston, A. L. (2001). Characterization of the AT4 receptor in a human neuroblastoma cell line (SK-N-MC). *J Neurochem* **76**:1679-1687.

Ofner, L., D. and Hooper, N., M. (2002). The C-terminus domain, but not the interchain disulphide, is required for the activity and intracellular trafficking of aminopeptidase A. *Biochem J* **362**:191-197.

Osada, T., Watanabe, G., Kondo, S., Toyoda, M., Sakaki, Y., Takeuchi, T. (2001b). Male reproductive defects caused by puromycin-sensitive aminopeptidase deficiency in mice. *Mol Endocrinol* 15: 960-971.

Osada, T., Watanabe, G., Sakaki, Y., Takeuchi, T. (2001a). Puromycin-sensitive aminopeptidase is essential for the maternal recognition of pregnancy in mice. *Mol Endocrinol* 15: 882-893.

Papadopoulos, T., Kelly, J. A. and Bauer, K. (2001). Mutational analysis of the thyrotropin-releasing hormone-degrading ectoenzyme. Similarities and differences with other members of the M1 family of aminopeptidases and thermolysin. *Biochem* **40**:9347-9355.

Peer, W. A., Hosein, F., N., Bandyopadhyay, A., Makam, S., N., Otegui, M., Lee, G., Blakeslee, J., J., Cheng, Y., Titapiwatanakun, B., Yakubov, B., Bangari, B., Murphy, A. S. (2009). Mutation of the membrane-associated M1 protease APM1 results in distinct embryonic and seedling developmental defects. *The Plant Cell* **21**:1693-721.

Pham VL, Cadel MS, Gouzy-Darmon C, Hanquez C, Beinfeld MC, Nicolas P, Etchebest C, Foulon T. (2007). Aminopeptidase B, a glucagon-processing enzyme: site directed mutagenesis of the Zn2+-binding motif and molecular modelling. BMC Biochem 8: 21-41.

Pfaffl, M.W. (2001) A new mathematical model for relative quantification in real-time RT-PCR. *Nucleic Acids Res* **29**: 2002-2007

Pradillo M, López E, Romero C, Sánchez-Morán E, Cuñado N, Santos JL. (2007). An analysis of univalent segregation in meiotic mutants of Arabidopsis thaliana: a possible role for synaptonemal complex. Genetics 175: 505-511.

Rozenfeld, R., Muller, L., Messari, S., E. and Llorens-Cortes, C. (2004). The C-terminal domain of aminopeptidase A is an intramolecular chaperone required for the correct folding, cell surface expression, and activity of this monozinc aminopeptidase. *J Biol Chem* **279**:43285-43295.

Rasmussen, T.E., Pedraza-Diaz, S., Hardre, R., Laustsen, P.G., Carrion, A.G., and Kristensen, T. (2000). Structure of the human oxytocinase/insulin-regulated aminopeptidase gene and localization to chromosome 5q21. *Eur J Biochem* **267**: 2297-2306.

Rost, B., Yachdav, G. and Liu, J. (2004). **The PredictProtein Server.** *Nucleic Acids Research* 32(Web Server issue):W321-W326.

Rudberg, P.C., Tholander, F., Thunnissen, M.M., and Haeggström, J.Z. (2002). Leukotriene A4 hydrolase/aminopeptidase. Glutamate 271 is a catalytic residue with specific roles in two distinct enzyme mechanisms. *J Biol Chem*. **277**: 1398-1404.

Sanchez-Moran, E., Jones, G., Franklin, F., and Santos, J. (2004). A puromycin-sensitive aminopeptidase is essential for meiosis in *Arabidopsis thaliana*. *Plant Cell* **16**: 2895-2909.

Smith AP, Nourizadeh SD, Peer WA, Xu J, Bandyopadhyay A, Murphy AS, Goldsbrough PB. (2003). Arabidopsis AtGSTF2 is regulated by ethylene and auxin, and encodes a glutathione S-transferase that interacts with flavonoids. Plant J 36: 433-442.

Titapiwatanakun, B., Blakeslee, J.J., Bandyopadhyay, A., Yang, H., Mravec, J., Sauer, M., Cheng, Y., Adamec, J., Nagashima, A., Geisler, M., Sakai, T., Friml, J., Peer, W.A.,

Murphy, A.S. (2009). ABCB19/PGP19 stabilises PIN1 in membrane microdomains in Arabidopsis. *Plant J*. **57**: 27-44

Towne, C.F., York, I.A., Neijssen, J., Karow, M.L., Murphy, A.J., Valenzuela, D.M., Yancopoulos, G.D., Neefjes, J.J., and Rock, K.L. (2008). Puromycin-sensitive aminopeptidase limits MHC class I presentation in dendritic cells but does not affect CD8 T cell responses during viral infections. *J Immunol.* **180**: 1704-1712.

Tsujimoto, M., Mizutani, S., Adachi, H., Kimura, M., Nakazato, H., and Tomoda, Y. (1992). Identification of human placental leucine aminopeptidase as oxytocinase. *Arch Biochem Biophys* **292**:388–392.

Vazeux, G., Iturrioz, X., Corvol, P., and Llorens-Cortes, C. (1998). A glutamate residue contributes to the exopeptidase specificity in aminopeptidase A. *Biochem. J.* **334**:407-413.

Walling, L.L. (2006). Recycling or regulation? The role of amino-terminal modifying enzymes. *Curr Opin Plant Biol*. **9**: 227-233.

Watson, R., T., Hou, J., C. and Pessin , J., E. (2008). Recycling of IRAP from the plasma membrane back to the insulin-responsive compartment requires the Q-SNARE syntaxin 6 but not the GGA adaptors. *J. Cell Sci.* **121**:1243-1251.

Wittig, I., Braun, H. and Sch□gger, H. (2006) Blue Native PAGE. *Nature Methods* **1**:418-428.

Ye, S., Chai, S.Y., Lew, R.A., Albiston, A.L. (2007). Insulin-regulated aminopeptidase: analysis of peptide substrate and inhibitor binding to the catalytic domain. *Biol Chem* 388: 399-403.

Zambrisky, P., Joos, H., Genetello, C., Leemans, J., van Montagu, M., and Schell, J. (1983). Ti plasmid vector for the introduction of DNA into plant cells without alteration of their normal regeneration capacity. *EMBO J*. **2:**2143–2150.

Table 1. Activity of recombinant APM1 *in vitro* translation product. Baseline is the activity of the *in vitro* translation of the empty vector control.

	nmol mg^{-1} min^{-1} (AFC[a], Ala or Tyr released)		
	DTT (mM)		
Peptide substrate	0	1	10
AlaGlyGly	36 ± 3.3	34 ± 5.7	31 ± 8.3
TyrGlyGly	40 ± 2.9	33 ± 6.4	32 ± 9.5
Ala-AFC	39 ± 7.2	38 ± 9.4	36 ± 11.3
Tyr-AFC	67 ± 5.1	70 ± 11.6	63 ± 14.8

[a] AFC = 7-amino-4-trifluoromethyl-coumarin

Table 2. Quantitative real-time PCR analysis of *APM1* expression in 5-d seedlings following NPA treatment. Data are means and standard deviations of five biological replicates.

	NPA (μM)			
	0	5	30	50
Relative abundance	8.5 ± 0.17	8.6 ± 0.28	9.7 ± 0.42*	11.7 ± 0.85*

*P < 0.05, ANOVA followed by Dunnet's post-hoc analysis.

Figure Legends

Figure 1. Phylogenetic analysis of M1 peptidases.

(A) Unrooted dendrogram of selected M1 peptidases from Animals, Archaea, and Plants. Peptidases are grouped according to sequence similarity to a representative of a given group. Protein sequences were aligned with MEGA 4.0 using an opening gap penalty of 10 and a gap extension penalty of 0.2. The neighbor-joining method of MEGA was used to construct the dendrogram with 1000 bootstrap replicates (indicated on branches). See Methods for more information. **(B) Schematic representation of selected M1 peptidases**. The characteristic M1 domains are highlighted: substrate recognition (GXMEN) and metal ion coordination domains (HEXXH) (dark grey), protein-protein interaction domain (medium grey), hydrophobic interaction domain which facilitates association to the membrane (light grey). The black bar represents a point mutation.

Figure 2. APM1 can form a dimer.

(A) Western blot of 10 µg whole microsomal membranes from 5-d wild type seedlings. Microsomal membranes were crosslinked with three different concentrations of BS^3, run on 8% SDS-PAGE, and incubated with α-APM1. **(B)** Western blot of 10 µg whole microsomal membranes prepared with and without a reducing agent (DTT), run on Blue Native PAGE and incubated with α-APM1. **(C)** Western blot of 10 µg *in vitro* translation of recombinant APM1 in rabbit recticulocytes, with and without NPA, analyzed via SDS-PAGE and incubated with α-APM1. **(D)** Western blot of 15 µg whole microsomal membranes from 5-d wild type seedlings treated with 0, 30 or 50 µM NPA, analyzed via Blue Native PAGE and incubated with α-APM1.

Figure 3. Alterations of the protein-protein interaction domain reduce phenotypic complementation. YFP-$APM1^{L729A}$ mutation is indicated by "LA" in the top cartoon, and YFP-$APM1^{\Delta 757\text{-}786}$ deletion is indicated by a black box in the bottom cartoon. **(A)** 5-d old wild type, *apm1-1* and YFP-$APM1^{L729A}$ seedlings germinated and grown on 10 µM Dex. **(B) – (D)** Confocal laser scanning microscopy (CLSM) analysis of YFP-$APM1^{L729A}$ **(B)** Autofluorescence control **(C)** Pro*35S*:YFP-APM1 **(D)** YFP-$APM1^{L729A}$ **(E)** Seed set of YFP-$APM1^{L729A}$ plants induced with 10 µM Dex. **(F)** 5-d old wild type, *apm1-1*, YFP-$APM1^{\Delta 757\text{-}786}$ seedlings germinated and grown on 10 µM Dex. **(G) – (I)** CLSM analysis of YFP-$APM1^{\Delta 757\text{-}786}$ (**G)**

autofluorescence **(H)** Pro*35S*:YFP-APM1 **(I)** YFP-APM1$^{\Delta 757\text{-}786}$ **(J)** Seed set of YFP-APM1$^{\Delta 757\text{-}786}$ plants induced with 10 µM Dex. Size bars: (A, F) 5mm; (E), (J) 5mm; (B- D), (G-I) 50 µm.

Figure 4. Catalytically inactive APM1 rescues *apm1-2* but not *apm1-1*.

(A) – (D) Complementation analyses of *apm1-1* with mutated catalytic residues. 5-d old seedlings. **(A)** *apm1-1* (+/-), **(B)** *apm1-1* (+/-) transformed with Pro*APM1*:APM1^{M273K} (M273K), **(C)** *apm1-1* (+/-) transformed with Pro*APM1*:APM1^{H307A} (H307A), **(D)** Seed set of wild type (WT) and mutants. **(E) – (L)** Complementation analyses of *apm1-2* (-/-) with mutated catalytic residues. **(E)** 5-d seedlings, **(F)** Gravitropic bending in *apm1-2* (-/-) transformed with Pro*APM1*:APM1^{M273K} (M273K) or Pro*APM1*:APM1^{H307A} (H307A), **(G)** Seed set, **(H)** 4 week old plants. **(I)** Western blot analyses of 10 µg whole microsomal membranes prepared from *apm1-2* 5-d seedlings expressing either Pro*APM1*:APM1^{M273K} or Pro*APM1*:APM1^{H307A} were crosslinked with 1 mM BS^3, run on 8% SDS-PAGE and incubated with anti-GFP. In the absence of BS^3, only monomers were observed (~105 kD). Size bars: (A-C) 1mm; (D) 15mm; (E, J) 1mm; (F- I) 1.5 cm; (K) 3 cm.

Figure 5. IRAP can rescue *apm1*.

(A)-(C) Phenotypic analyses of *apm1-1*(+/-) transformed with IRAP or the catalytically inactive IRAPm. **(A)** 5-d old seedlings, **(B)** 3 week old plants, **(C)** Seed set **(D)-(F)** Phenotypic analyses of *apm1-2* (-/-) transformed with IRAP or the catalytically inactive IRAPm. **(D)** 5-d old seedlings, **(E)** 3 week old plants, **(F)** Seed set. Size bars: (A, D) 5mm; (B, E) 3cm; (C, F) 5mm.

Figure 6. Membrane association of APM1 is important for its function.

(A) 5-d old seedlings of wild type, *apm1-1* (+/-), APM1$^{\Delta 98\text{-}205}$ **(B) – (D)** Localization of APM1$^{\Delta 98\text{-}205}$**(B)** Autofluorescence control **(C)** Pro*35S*:YFP-APM1 **(D)** Pro*35S*:YFP-APM1$^{\Delta 98\text{-}205}$ **(E)** Seed set of wild type, *apm1-1* (+/-), and Pro*35S*:YFP-APM1$^{\Delta 98\text{-}205}$, **(F)** Gravitropic response. Size bars: (A) 5mm; (B-D) 50 µm; (E) 5mm.

A

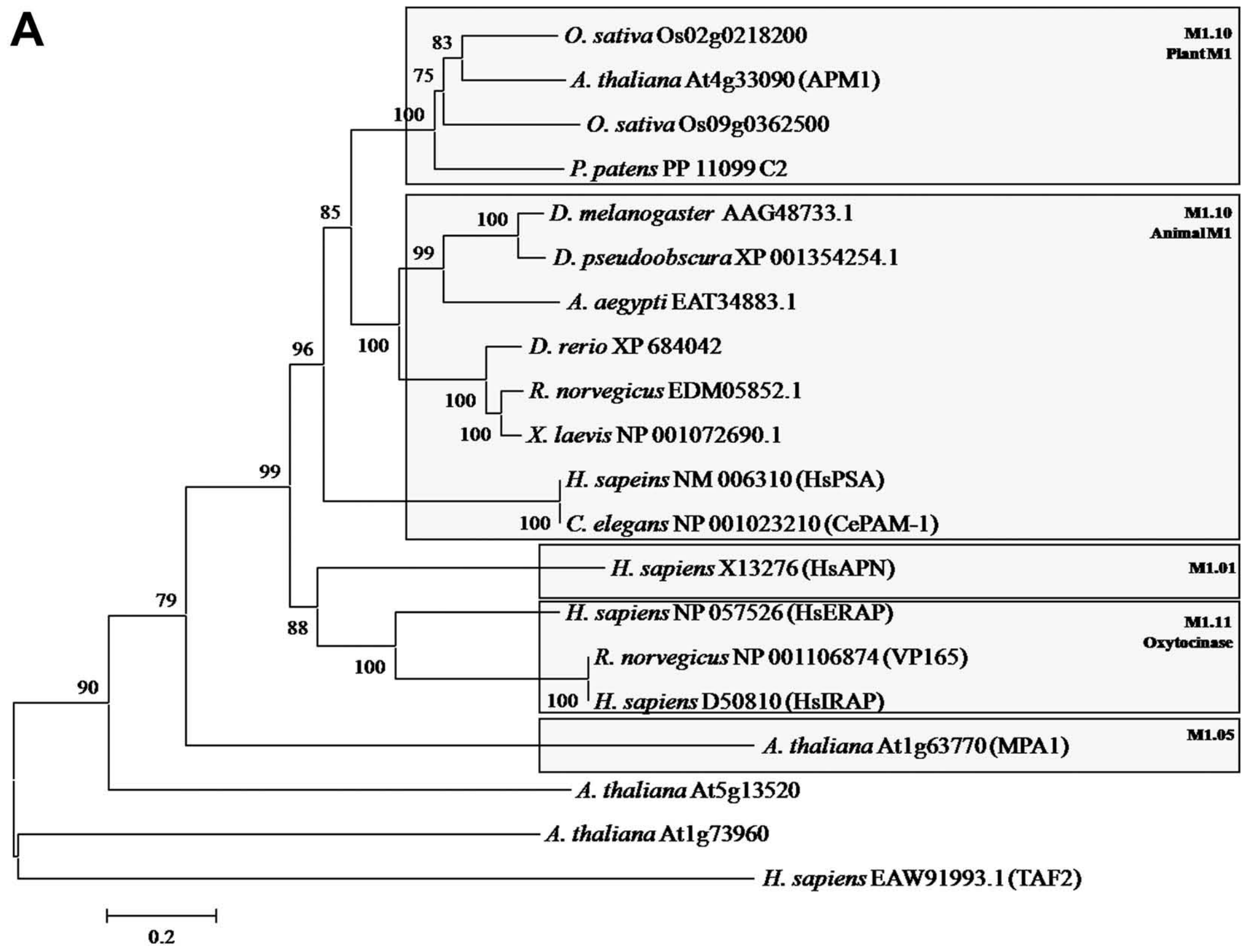

B

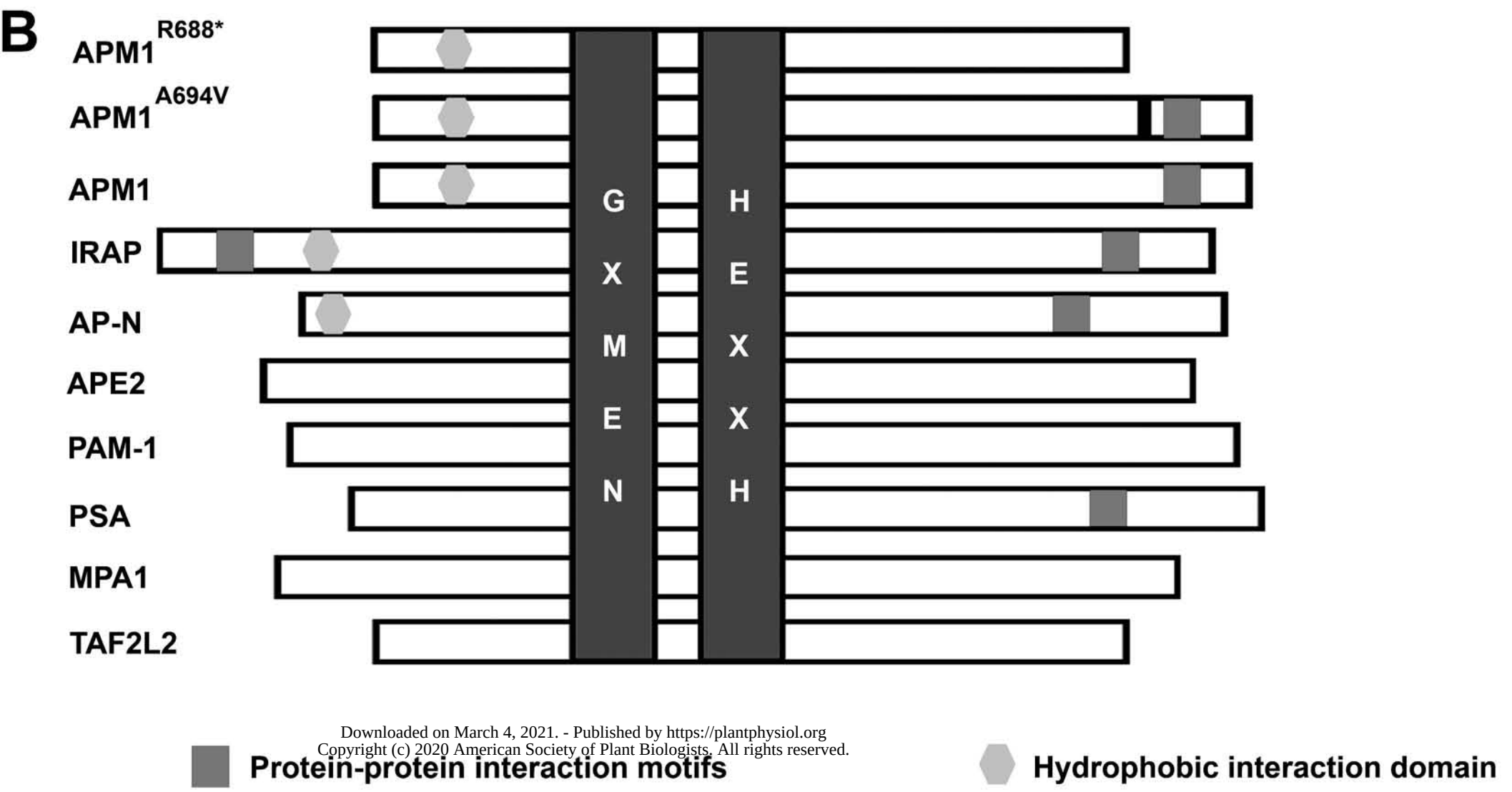

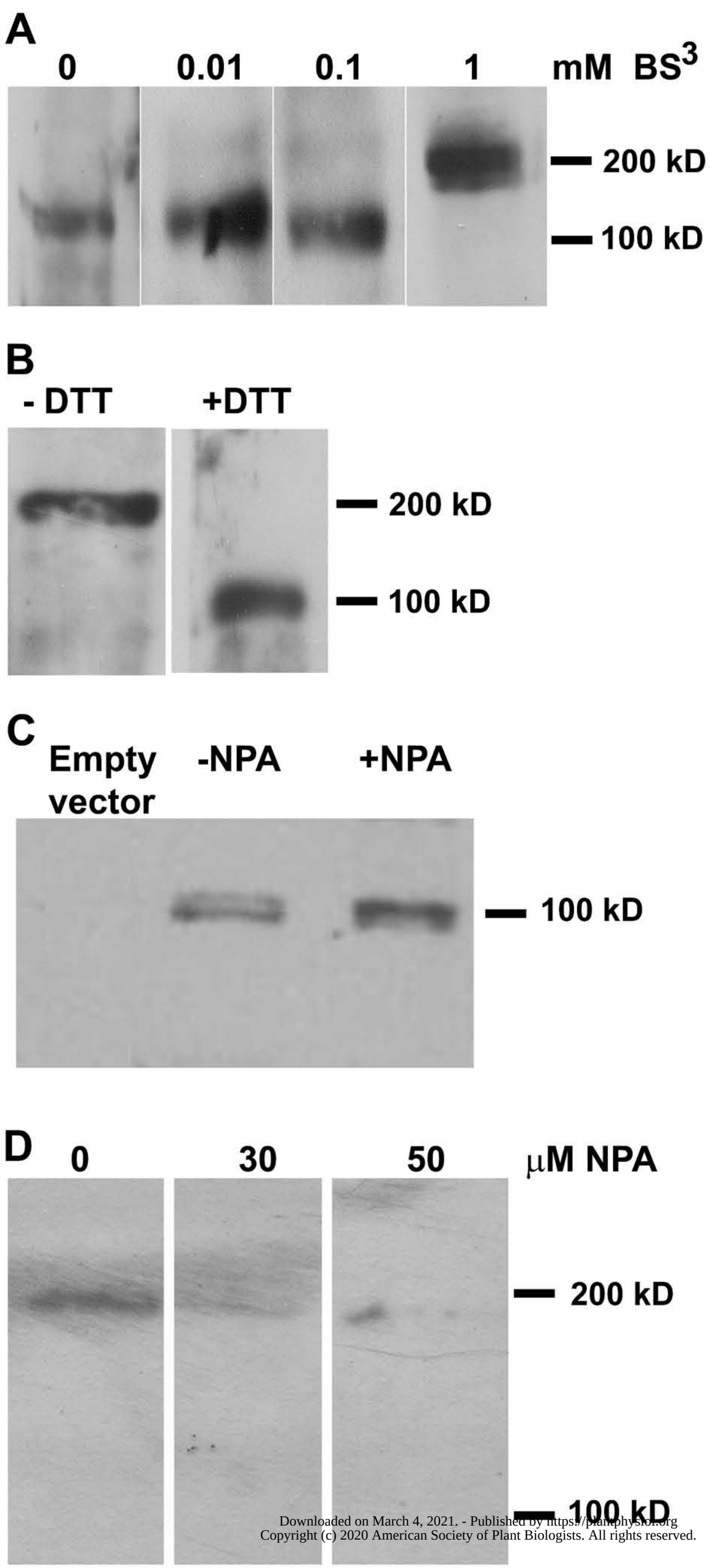

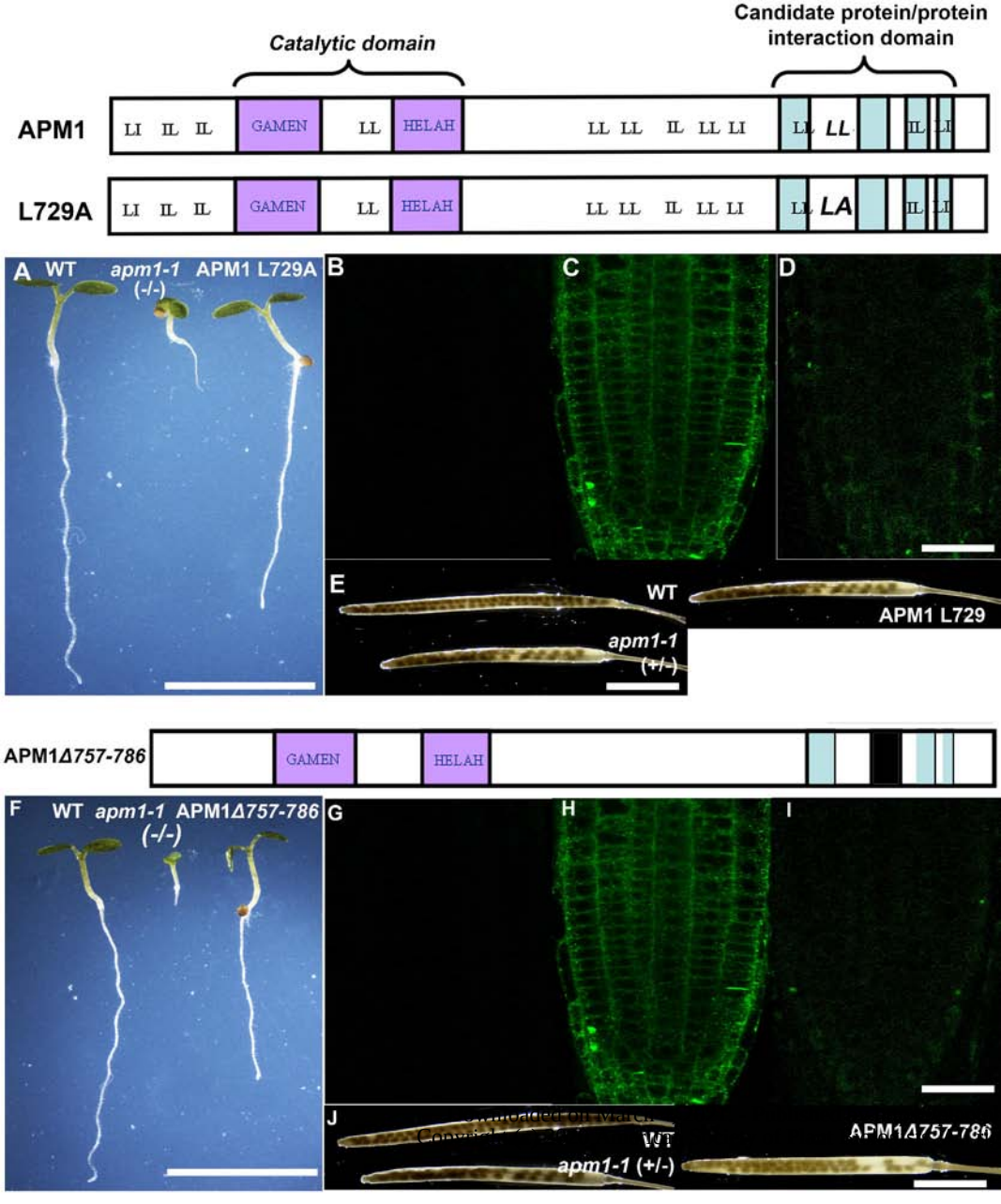
Catalytic domain
Candidate protein/protein interaction domain
APM1
LI IL IL
GAMEN
LL
HELAH
LL LL IL LL LI
LL LL
IL LI
L729A
LL LA
A WT
apm1-1 (-/-)
APM1 L729A
B
C
D
E
WT
APM1 L729
apm1-1 (+/-)
APM1Δ757-786
F WT apm1-1 (-/-) APM1Δ757-786
G
H
I
J
WT
apm1-1 (+/-)
APM1Δ757-786